Optimization of Spatial Resolution for Peripheral Magnetic Resonance Angiography[1]

An Tang, Guy Cloutier, Eric Therasse, Gilles Beaudoin, Salah D. Qanadli, Marie-France Giroux, Nicolas Boussion
Jacques A. de Guise, Vincent L. Oliva, Gilles Soulez

Rationale and Objectives. To determine optimum spatial resolution when imaging peripheral arteries with magnetic resonance angiography (MRA).

Materials and Methods. Eight vessel diameters ranging from 1.0 to 8.0 mm were simulated in a vascular phantom. A total of 40 three-dimensional flash MRA sequences were acquired with incremental variations of fields of view, matrix size, and slice thickness. The accurately known eight diameters were combined pairwise to generate 22 "exact" degrees of stenosis ranging from 42% to 87%. Then, the diameters were measured in the MRA images by three independent observers and with quantitative angiography (QA) software and used to compute the degrees of stenosis corresponding to the 22 "exact" ones. The accuracy and reproducibility of vessel diameter measurements and stenosis calculations were assessed for vessel size ranging from 6 to 8 mm (iliac artery), 4 to 5 mm (femoro-popliteal arteries), and 1 to 3 mm (infrapopliteal arteries). Maximum pixel dimension and slice thickness to obtain a mean error in stenosis evaluation of less than 10% were determined by linear regression analysis.

Results. Mean errors on stenosis quantification were 8.8% ± 6.3% for 6- to 8-mm vessels, 15.5% ± 8.2% for 4- to 5-mm vessels, and 18.9% ± 7.5% for 1- to 3-mm vessels. Mean errors on stenosis calculation were 12.3% ± 8.2% for observers and 11.4% ± 15.1% for QA software ($P = .0342$). To evaluate stenosis with a mean error of less than 10%, maximum pixel surface, the pixel size in the phase direction, and the slice thickness should be less than 1.56 mm^2, 1.34 mm, 1.70 mm, respectively (voxel size 2.65 mm^3) for 6- to 8-mm vessels; 1.31 mm^2, 1.10 mm, 1.34 mm (voxel size 1.76 mm^3), for 4- to 5-mm vessels; and 1.17 mm^2, 0.90 mm, 0.9 mm (voxel size 1.05 mm^3) for 1- to 3-mm vessels.

Conclusion. Higher spatial resolution than currently used should be selected for imaging peripheral vessels.

Key Words. Magnetic resonance angiography; peripheral arteries; experimental studies.

Magnetic resonance angiography (MRA) has gained widespread clinical acceptance for imaging the aorta and its major branches (1–4). Technical advances in contrast-enhanced bolus chase three-dimensional (3D)-MRA with fast-gradient echo-recalled sequences, moving table, and time-resolved imaging have improved diagnostic accuracy (5–11).

However, suboptimal correlations with Digital subtraction angiography (DSA) have often been reported because of limited spatial resolution and frequent venous contamination observed with the sequence used for bolus-chasing MRA (12,13). For infrapopliteal vessels, better results have been obtained when the examination was performed in two steps: a first injection combined with high-resolu-

Acad Radiol 2007; 14:54–61

[1] From the Department of Radiology (A.T., E.T., G.B., M.-F.G., V.L.O., G.S.), the Laboratory of Biorheology and Medical Ultrasonics-Research Center (G.C., N.B.), and Laboratory of Orthopedic Imaging-Research Center (J.D.G.), Centre Hospitalier de l'Université de Montréal (CHUM)-Hôpital Notre-Dame, Montreal, Quebec, Canada; and the Department of Radiology, Centre Hospitalier Universitaire Vaudois, Lausanne, Switzerland (S.D.Q.). Received March 6, 2006; accepted October 13, 2006. Supported by grants from the Canadian Institutes of Health Research (G.C., G.S.; #MOP-53244) and Valorisation-Recherche Québec (group grant #2200-094), and by a National scientist award (G.C.) and clinical research scholarship awards from Fonds de la recherche en santé du Québec (G.C., G.S.). **Address correspondence to:** G.S. e-mail: gilles.soulez.chum@ssss.gouv.qc.ca

doi:10.1016/j.acra.2006.10.007

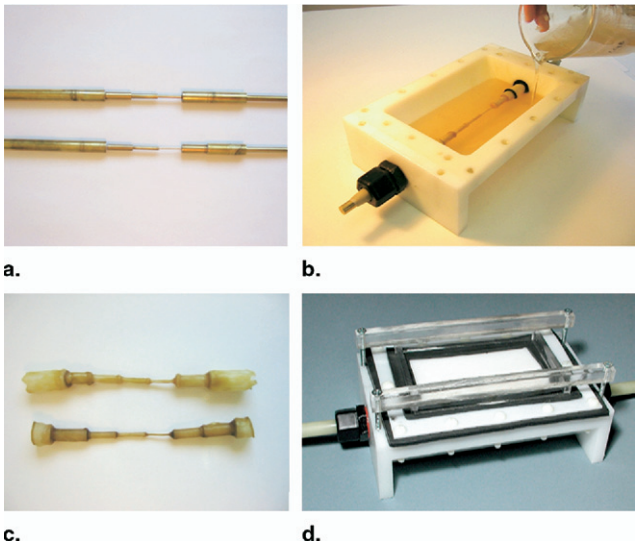

Figure 1. Phantom construction using lost-material casting technique. (a) Two bronze rods with segment diameters ranging from 1.0 to 8.0 mm. (b) Filling of vascular phantom with tissue-mimicking agar-based gel. (c) Latex vessels after removal of rod-latex unit. (d) Multimodality vascular phantom. Outer view.

tion acquisition on the distal leg and foot followed by a second injection to image proximal vessels (14). However, this approach requires two consecutive injections and acquisitions to image the entire runoff.

To the best of our knowledge, no study has assessed the minimal spatial resolution when imaging iliac, femoropopliteal, and infrapopliteal arteries by gadolinium-enhanced MRA. Also, the best tradeoff between spatial resolution and acquisition time for bolus-chasing MRA needs to be defined to avoid motion artifacts, minimize venous enhancement (15), and exploit a single contrast-bolus injection combined with the moving-bed technique (16).

The aim of this study was to establish the optimum voxel dimension for the three acquisitions undertaken in peripheral runoff studies: aorto-iliac, femoropopliteal, and infrapopliteal vessels.

MATERIALS AND METHODS

Vascular Phantoms

Two multimodality vascular phantoms were built to simulate vessels of size comparable to those of lower limb arteries (17). We simulated the process of stenosis measurement by combining different lumen diameters, rather than physically simulate stenoses per se.

With a lost-material casting technique (18,19), we applied a 1-mm thin latex layer simulating a vessel wall around a cylindrical bronze rod made of four adjacent 20-mm long pieces with different diameters (Fig 1). Two phantoms were built, one with segment diameters of 7.91, 6.29, 4.39, 2.39, and 0.99 mm, and the other with segment diameters of 5.10, 3.21, and 1.87 mm. The accurately known eight diameters were combined pairwise to generate 22 "exact" degrees of stenosis ranging from 42% to 87% (Table 1).

Table 1
Pairs of Vessels and Corresponding Exact Degrees of Stenosis for the Stations "Infrapopliteal," "Femoropopliteal," and "Iliac"

Level	Pairs of Vessels (mm/mm)	Stenosis Percentage (%)
Infrapopliteal	1.87/3.21	41.74
(1- to 3-mm vessels)	0.99/1.87	47.06
	0.99/2.39	58.58
	0.99/3.21	69.16
Femoropopliteal	3.21/5.10	37.06
(4- to 5-mm vessels)	2.39/4.39	45.56
	2.39/5.10	53.14
	1.87/4.39	57.40
	1.87/5.10	63.33
	0.99/4.39	77.45
	0.99/5.10	80.59
Iliac	4.39/6.29	30.21
(6- to 8-mm vessels)	5.10/7.91	35.52
	4.39/7.91	44.50
	3.21/6.29	48.97
	3.21/7.91	59.42
	2.39/6.29	62.00
	2.39/7.91	69.79
	1.87/6.29	70.27
	1.87/7.91	76.36
	0.99/6.29	84.26
	0.99/7.91	87.48

The rod-latex unit was then molded in a tissue-mimicking, agar-based gel inside a polyethylene phantom frame. After the agar solidified, the rod was removed, letting us a vascular conduit of known geometry that was connected to tubings at its extremities.

The lumen of the latex vessel was filled with gadolinium solution (gadopentate dimeglumine, Magnevist; Berlex Canada, Lachine, Quebec, Canada) of 1.8 mmol/L diluted with 0.9% NaCl solution with concentration comparable to that of a bolus (20,21). The vessel lumen was maintained in static conditions with a constant 100-mm Hg lumen pressure to avoid vessel collapse (17). The accuracy and precision of phantom lumen diameters in these conditions were estimated previously at -0.004×0.18 mm (17).

Table 2
Pixel Dimensions for All Magnetic Resonance Angiography Acquisition Parameters

Acquisition #	Field of View (mm)	Matrix Size	Pixel Size (mm × mm)	Slice Thickness (mm)	Voxel Size (mm^3)
1	390 × 390	512 × 410	0.76 × 0.95	1.31	0.95
2	390 × 390	512 × 410	0.76 × 0.95	1.50	1.08
3	390 × 390	512 × 410	0.76 × 0.95	2.00	1.44
4	390 × 390	512 × 410	0.76 × 0.95	2.50	1.81
5	390 × 390	512 × 410	0.76 × 0.95	3.00	2.17
6	390 × 390	512 × 320	0.76 × 1.22	1.31	1.21
7	390 × 390	512 × 320	0.76 × 1.22	1.50	1.39
8	390 × 390	512 × 320	0.76 × 1.22	2.00	1.85
9	390 × 390	512 × 320	0.76 × 1.22	2.50	2.31
10	390 × 390	512 × 320	0.76 × 1.22	3.00	2.78
11	390 × 390	512 × 260	0.76 × 1.50	1.31	1.49
12	390 × 390	512 × 260	0.76 × 1.50	1.50	1.71
13	390 × 390	512 × 260	0.76 × 1.50	2.00	2.28
14	390 × 390	512 × 260	0.76 × 1.50	2.50	2.85
15	390 × 390	512 × 260	0.76 × 1.50	3.00	3.42
16	390 × 390	256 × 190	1.52 × 2.05	1.31	4.08
17	390 × 390	256 × 190	1.52 × 2.05	1.50	4.67
18	390 × 390	256 × 190	1.52 × 2.05	2.00	6.23
19	390 × 390	256 × 190	1.52 × 2.05	2.50	7.79
20	390 × 390	256 × 190	1.52 × 2.05	3.00	9.35
21	490 × 490	512 × 410	0.96 × 1.20	1.31	1.51
22	490 × 490	512 × 410	0.96 × 1.20	1.50	1.73
23	490 × 490	512 × 410	0.96 × 1.20	2.00	2.30
24	490 × 490	512 × 410	0.96 × 1.20	2.50	2.88
25	490 × 490	512 × 410	0.96 × 1.20	3.00	3.46
26	490 × 490	512 × 320	0.96 × 1.53	1.31	1.92
27	490 × 490	512 × 320	0.96 × 1.53	1.50	2.20
28	490 × 490	512 × 320	0.96 × 1.53	2.00	2.93
29	490 × 490	512 × 320	0.96 × 1.53	2.50	3.67
30	490 × 490	512 × 320	0.96 × 1.53	3.00	4.41
31	490 × 490	512 × 260	0.96 × 1.88	1.31	2.36
32	490 × 490	512 × 260	0.96 × 1.88	1.50	2.71
33	490 × 490	512 × 260	0.96 × 1.88	2.00	3.61
34	490 × 490	512 × 260	0.96 × 1.88	2.50	4.51
35	490 × 490	512 × 260	0.96 × 1.88	3.00	5.41
36	490 × 490	256 × 190	1.91 × 2.58	1.31	6.46
37	490 × 490	256 × 190	1.91 × 2.58	1.50	7.39
38	490 × 490	256 × 190	1.91 × 2.58	2.00	9.86
39	490 × 490	256 × 190	1.91 × 2.58	2.50	12.32
40	490 × 490	256 × 190	1.91 × 2.58	3.00	14.78

Note: All other acquisition parameters remained constant: time of repetition 4.6/time of echo 1.8/flip angle 30°/number of excitation 1.

Description of the System and Acquisition Protocols

A 1.5-Tesla magnet (Magnetom Vision; Siemens, Erlangen, Germany) and a body array coil were used for the phantom study. The phantom with simulated vessel segments was positioned parallel to B_0. Forty 3D, fast, low angle shot (3D Flash) MRA acquisitions were performed in the coronal plane with two different fields of views (390 × 390 mm and 490 × 490 mm), four different matrix sizes (512 × 410, 512 × 320, 512 × 260, 256 × 190), and five different slice thicknesses (1.31, 1.50, 2.00, 2.50, 3.00 mm). The pixel and voxel sizes used in the acquisitions are detailed in Table 2. No pixel interpolation was used. All other parameters remained constant: time of repetition/time of echo 4.6/1.8; flip angle 30°; number of excitation 1; slab thickness 70 mm.

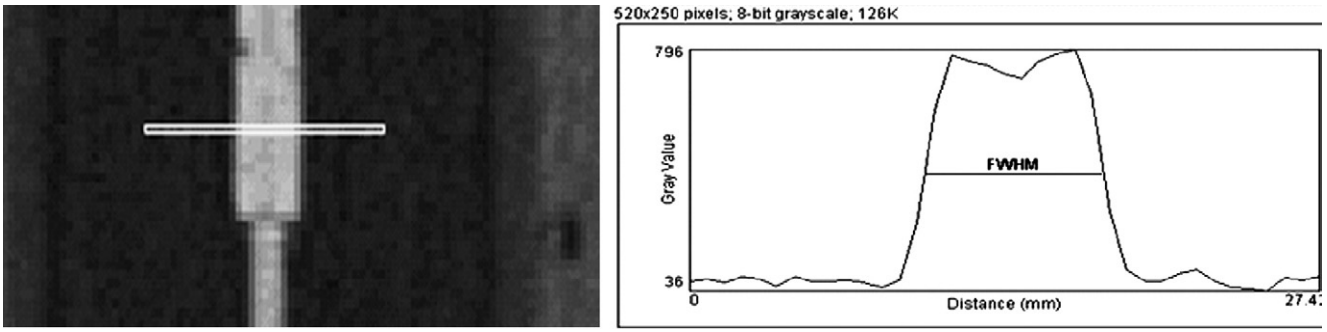

Figure 2. Quantitative automated measurement technique. (a) Image shows a coronal view of the vascular phantom with a transverse line perpendicular to the vessel axis indicating the measurement level. (a) Signal intensity along the transverse line in the left panel. The quantitative diameter measurement corresponds to full width of half the maximum intensity (full width at half maximum technique).

Description of the Measurement Protocols

For each acquisition, one two-dimensional coronal source image and one coronal and one sagittal maximum intensity projection images were generated on a 3D viewing workstation (3D Virtuoso; Siemens). Each generated image included eight segments of different diameters acquired with the same acquisition parameters. This resulted in 960 segments (40 acquisitions × 3 images/acquisition × 8), which were independently measured by three experienced vascular radiologists and by a quantitative angiography (QA) system and used to compute the degrees of stenosis corresponding to the 22 "exact" ones.

Diameter measurements by these radiologists were taken using standardized reading parameters (window width: 912; window level: 473; magnification: 4.0×) on a PACS workstation (IMPAX 3.5; Agfa Medical Imaging, Greenville, SC). The radiologists positioned electronic calipers at vessel borders perpendicularly to the long axis of the vessel. Objective image analysis was performed with a public domain software (NIH Image J, version 1.27z; National Institute of Health, Bethesda, MD) that allows QA measurements using an intensity profile as the width at middle height of the peak of intensity (full width at half maximum technique) (Fig 2). This technique allows window-setting independent measurements (22,23).

Statistical Analyses of Phantom Study

Individual measurements of lumen diameters taken at the mid-portion of each vessel segment were compared with true phantom diameters. Segment vessels deemed too blurred to be measured were excluded for vessel diameter analysis, and the error of stenosis quantification was arbitrarily set at 100% for these segments.

Signed mean errors, which are the mean of signed absolute differences (in percent) between measured values and the known diameters or known degree of stenoses, were calculated with their standard deviation and confidence intervals. Each radiologist's dataset was analyzed individually; the individual results were then averaged. Intraclass correlation coefficients between the radiologists and QA measurements were computed for diameter measurement and stenosis calculation.

Paired Student *t*-test was applied to underline differences between radiologists and QA measurements.

In addition, linear regression analysis with calculations of Pearson's correlation coefficients was performed to assess the correlations between mean errors of stenosis estimation and pixel width, surface, and slice thickness. Mean measurements of coronal source and coronal maximum intensity projection images served to assess the correlations of these errors with the pixel surface or spatial resolution in the phase direction, whereas sagittal maximum intensity projection measurements were used to assess the correlation for slice thicknesses.

Based on the results of the linear regression analyses, we calculated hypothetical thresholds for maximal pixel size in the phase direction, pixel surface, and slice thickness when a 90% accuracy in stenosis measurement is required (mean error inferior to 10%). Although arbitrary, these accuracy thresholds were deemed to be clinically acceptable to provide the physician information for therapeutic planning. These evaluations of stenosis measurements were performed separately for the diameters ranging from 6 to 8, 4 to 5, and 1 to 3 mm because we wanted to take into account the three usual steps of peripheral MRA acquisition (aorto-iliac, femoropopliteal,

Table 3
Mean Error and Precision of Diameter Measurements and Stenosis Estimation for All Sequences

	Diameters			Stenoses		
Observers	Mean Error (mm)	Precision (1 SD)	Confidence Interval	Mean Error (%)	Precision (1 SD)	Confidence Interval
QA software	−0.083	±0.827	−0.138/−0.030	11.4	±15.1	10.3/12.5
Average 3 radiologists	+1.130	±0.764	+1.081/+1.180	12.3	±8.2	11.7/12.9
ICC for 4 observers		0.8304			0.7632	
Difference between software and radiologists		Mean = 1.21 ± 0.89 mm P <.0001			Mean = 0.9 ± 0.12% P = .034	

SD: standard deviation; QA: quantitative angiography; ICC: intra-class correlation coefficient.

and infrapopliteal). The obtained thresholds yield the optimal pixel dimensions.

Mean errors of diameter and stenosis measurements of the three observers and QA were recalculated, with measurements taken only on acquisitions having a spatial resolution equivalent to or higher than the previously defined thresholds.

In all cases, statistical analysis was performed with commercially available software (SAS version 8.2, SAS Institute Inc, Cary, NC).

RESULTS

Diameter Measurements

Each observer performed 960 diameter measurements. Of a total of 3,840 diameters, 109 images were deemed too blurred to be measured by the radiologists or returned aberrant values with QA software. Mean errors on diameter measurement were smaller with QA software (−0.08 ± 0.83 mm) than for the radiologists (+1.13 ± 0.76 mm) ($P < .0001$) (Table 3). The reproducibility of the measurements in the phantom between the group of three observers and QA software was very good, as revealed by a global intraclass correlation coefficient (ICC) of 0.83.

Stenosis Calculations

Pairing the diameters generated 880 measures of stenoses. Of a total of 3,520 potential stenoses for four observers, 341 were not valid because one of the two diameters was nonmeasurable.

Stenosis overestimation was observed with both manual and automated measurements (Table 3). Mean errors on stenosis calculation were also higher for the three radiologists (12.3% ± 8.2%) than for QA software (11.4% ± 15.1%) ($P = .0342$). Reliability among the three observers and QA software was good, with a global ICC of 0.76.

Table 4
Stenosis Quantification by Radiologists/by Vessel Size for All Acquisitions

	Stenoses		
Vessel Size	Mean Error (%)	Precision (1 SD)	Confidence Interval
1–3 mm	19.0	±7.6	17.5/20.5
4–5 mm	15.6	±8.2	14.5/16.6
6–8 mm	8.8	±6.3	8.1/9.4
ICC for stenoses measurements		1–3 mm = 0.5761 4–5 mm = 0.6697 6–8 mm = 0.7755	

SD: standard deviation; ICC: intraclass correlation coefficient.

Stenosis quantification by the radiologists was more accurate for larger than for smaller vessels, with an overall accuracy of 8.8% ± 6.3% (SD) for 6- to 8-mm vessels, 15.5% ± 8.2% for 4- to 5-mm vessels, and 18.9% ± 7.5% for 1- to 3-mm vessels (Table 4).

Effect of Spatial Resolution in the Phase Direction

Regression analysis of the mean errors on stenosis measurement and spatial resolution in the phase direction (pixel width) is detailed for the three different vessel sizes in Fig 3. Our results show that the correlation between mean errors on stenosis measurement and spatial resolution in the phase direction was significant for all vessel sizes, but higher for smaller vessels: $r = 0.538$ for 1- to 3-mm vessels ($P < .0001$); $r = 0.471$ for 4- to 5-mm vessels ($P < .0001$); and $r = 0.365$ for 6- to 8-mm vessels ($P < .001$).

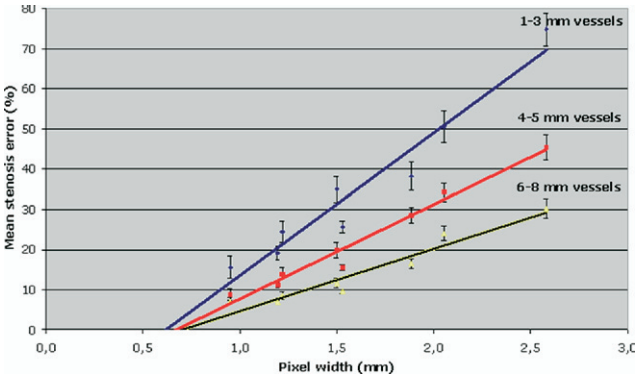

Figure 3. Regression analysis of mean errors of the measured degrees of stenosis versus pixel width (mm) for the three vessel size ranges. The pixel width is the spatial resolution defined by the matrix size in the phase direction. Bars represent standard error of the means.

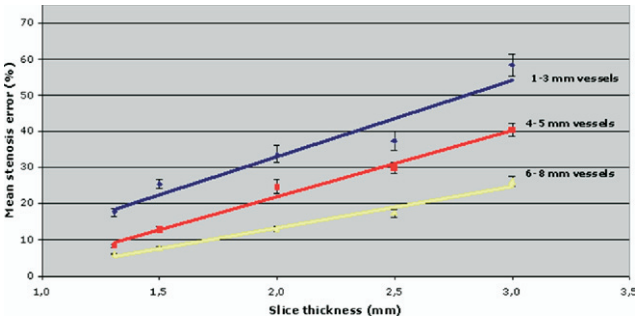

Figure 4. Regression analysis of mean errors on the measured degrees of stenosis (%) versus slice thickness (mm) for the three vessel size ranges. Bars represent standard error of the means.

Effect of Pixel Size

Slightly lower but still highly significant correlation coefficients were found by regression analysis between the mean errors on stenosis measurement and pixel size (pixel surface): $r = 0.4666$ for 1- to 3-mm vessels ($P < .0001$); $r = 0.3730$ for 4- to 5-mm vessels ($P < .0001$); and $r = 0.2877$ for 6- to 8-mm vessels ($P < .001$).

Effect of Slice Thickness

Linear regression analysis between the mean error on stenosis and slice thickness is presented in Fig 4. The correlation was also stronger for small vessel diameters and significant for all vessel sizes: for 1- to 3-mm vessels, $r = 0.4501$ ($P < .0001$); for 4- to 5-mm vessels, $r = 0.4816$ ($P < .0001$); and for 6- to 8-mm vessels, $r = 0.3843$ ($P < .001$).

According to these statistical results, a mean stenosis measurement error below 10% was obtained for 6- to 8-mm vessels by using a maximal pixel size in the phase direction of 1.34 mm, pixel surface of 1.56 mm^2, and slice thickness of 1.70 mm (voxel size 2.65 mm^3); for 4- to 5-mm vessels, a maximum pixel size in the phase direction of 1.10 mm, pixel surface of 1.31 mm^2, and slice thickness of 1.34 mm (voxel size 1.76 mm^3). To achieve the same level of accuracy with 1- to 3-mm vessels, it was extrapolated from the same regression analyses equations that a maximum pixel size in the phase direction of 0.90 mm, a pixel surface of 1.17 mm^2, and a slice thickness of 0.90 mm would be required (voxel size 1.05 mm^3).

Table 5
Stenosis Quantification by Radiologists/by Vessel Size After Sequence Selection

	Stenoses		
Vessel size	Mean Error (%)	Precision (1 SD)	Confidence Interval
1–3 mm	8.7	±4.0	2.3/15.0
4–5 mm	8.4	±5.6	5.9/10.9
6–8 mm	6.2	±4.1	5.3/7.1
ICC for stenoses		1–3 mm = 0.7241	
		4–5 mm = 0.7721	
		6–8 mm = 0.8584	

SD: standard deviation; ICC: intraclass correlation coefficient.

Improvement in the accuracy and precision of stenosis evaluations was observed when only sequences having a spatial resolution equivalent to or higher than the thresholds previously defined were chosen (1.5% ± 7.0% for QA software and 6.7% ± 4.5% for the three radiologists) with a very good reproducibility between the group of three observers and QA software (ICC of 0.84) (Table 5).

DISCUSSION

Lower extremity peripheral vessels are commonly acquired in the coronal (XZ) rather than the axial (XY) plane to maximize the spatial resolution in the coronal plane, which is important in imaging lower limb vessels. Because stenoses are perpendicular to the vessel axis, stenosis severity would be better evaluated in the XY plane for most of the peripheral vessels.

In this study, we have found a proportional relationship between mean stenosis error versus spatial resolution in the phase direction, pixel surface, and slice thickness. This work demonstrates also that higher spatial resolution than presently used in clinical practice is necessary to

properly image lower limb arteries in peripheral MRA, even at the level of iliac and femoral arteries. Pixel dimensions currently used for peripheral runoff studies are too large for the vessel diameter to be measured especially at the infrapopliteal level. This study also showed that an optimal combination of smaller pixel dimensions in the x, y, and z axes improved the accuracy and precision of stenosis measurements.

Our phantom study revealed a slight overestimation of vessel diameter when assessed by the radiologists. Stenoses were overestimated by all three observers and by the QA software. This effect was more pronounced on small than large vessel diameters, as reported previously (24). In the literature, stenosis overestimation has been often reported with Gd-enhanced MRA (7,11,14).

We demonstrated better accuracy and interobserver variability on measurement with QA software over manual measurement by an independent observer, both for diameter and stenosis assessments. Overestimation of diameters by the radiologists can be explained by perception issues. Conversely, quantitative automated measurements are window-independent and rely on plot profiles of source magnetic resonance imaging signals (22). However, the accuracy of this method can be influenced by saturation effects.

Obtaining the level of spatial resolution recommended by our phantom study during a three-station examination while avoiding venous contamination requires MRA equipment with high gradient capabilities, time-resolved imaging, and a dedicated phased array coil. Recently, advances in gradient technology have shortened the minimal time of repetition. However, even with last-generation equipment, it is not possible to get this level of spatial resolution using conventional 3D-Flash sequences.

The 3D "shoot-and-scoot" techniques involving central k-space acquisition during bolus injection followed by peripheral k-space acquisition during the venous phase could be another alternative to obtain this level of spatial resolution while minimizing venous superposition (25).

Another alternative is to use parallel acquisition techniques [SiMultaneous Acquisition of Spatial Harmonics (SMASH), SENSitivity Encoding (SENSE), GeneRalized Autocalibrating Partially Parallel Acquisition (GRAPPA)] and to shorten scan time by a factor proportional to the parallel imaging factor. De Vries et al and Bezooijen et al have used a parallel imaging factor of 2 with satisfactory clinical results (8,9). However, the voxel dimension used in their studies was larger than the maximum voxel size defined in our study (5.3 mm^3, 4.3–3.9 mm^3, and 1.4–0.98 mm^3 at the pelvic, upper, and lower leg stations, respectively). In a clinical setting, we tried to implement on an Avanto unit (Siemens, Erlangen) acquisitions parameters for peripheral runoff examinations to get a spatial resolution higher or equivalent to the thresholds defined in our study. To fit these parameters within an acquisition time inferior to 70 seconds, we had to apply a GRAPPA factor of 3. This gain in time of acquisition and spatial resolution is made at the price of additional artifacts and loss of signal-to-noise ratio, which can deteriorate image quality (26,27).

Study Limitations

This study was performed in ideal conditions with a vessel phantom parallel to the magnetic field (B_0) that did not take into account the obliquity of the iliac bifurcation and popliteal trifurcation. Also, the effects of flow and pulsatility were not included. We have not measured stenosis within vessels, but we have simulated stenoses by combining diameter ratios. Atherosclerotic stenoses are often irregular, eccentric, and more difficult to evaluate. At the time this phantom study was conducted, parallel imaging was not available in our institution; therefore, optimized pixel dimension have been set only with conventional 3D-Flash sequences.

Based on our phantom study, we can conclude that higher spatial resolution than currently used in clinical routine should be selected to image peripheral arteries and that quantitative automated analysis of vessel diameter and stenosis is more accurate than manual measurements.

REFERENCES

1. Meaney JF, Ridgway JP, Chakraverty S. Stepping-table gadolinium-enhanced digital subtraction MR angiography of the aorta and lower extremity arteries: preliminary experience. Radiology 1999; 211:59–67.
2. Rofsky NM, Adelman MA. MR angiography in the evaluation of atherosclerotic peripheral vascular disease, Radiology 2000; 214:325–338.
3. Nelemans P, Leiner T, de Vet HCW, et al. Peripheral arterial disease: meta-analysis of the diagnostic performance of MR angiography. Radiology 2000; 217:105–114.
4. Koelemay MJ, Lijmer JG, Stoker J, et al. Magnetic resonance angiography for the evaluation of lower extremity arterial disease: a meta-analysis. JAMA 2001; 285:1338–1345.
5. Steffens JC, Schafer FK, Oberscheid B, et al. Bolus-chasing contrast-enhanced 3D MRA of the lower extremity. Comparison with intraarterial DSA. Acta Radiol 2003; 44:185–192.
6. Vavrik J, Rohrmoser GM, Madani B, et al. Comparison of MR angiography versus digital subtraction angiography as a basis for planning treatment of lower limb occlusive disease. J Endovasc Ther 2004; 11: 294–301.
7. Loewe C, Schoder M, Rand T, et al. Peripheral vascular occlusive disease: evaluation with contrast-enhanced moving-bed MR angiography versus digital subtraction angiography in 106 patients. AJR Am J Roentgenol 2002; 179:1013–1021.
8. Bezooijen R, van den Bosch HC, Tielbeek AV, et al. Peripheral arterial disease: sensitivity-encoded multiposition MR angiography compared

with intraarterial angiography and conventional multiposition MR angiography. Radiology 2004; 231:263–271.
9. de Vries M, Nijenhuis RJ, Hoogeveen RM, et al. Contrast-enhanced peripheral MR angiography using SENSE in multiple stations: feasibility study. J Magn Reson Imaging 2005; 21:37–45.
10. Leiner T, Kessels AG, Schurink GW, et al. Comparison of contrast-enhanced magnetic resonance angiography and digital subtraction angiography in patients with chronic critical ischemia and tissue loss. Invest Radiol 2004; 39:435–444.
11. Hentsch A, Aschauer MA, Balzer JO, et al. Gadobutrol-enhanced moving-table magnetic resonance angiography in patients with peripheral vascular disease: a prospective, multi-centre blinded comparison with digital subtraction angiography. Eur Radiol 2003; 13:2103–2114.
12. Klein WM, Schlejen PM, Eikelboom BC, et al. MR angiography of the lower extremities with a moving-bed infusion-tracking technique. Cardiovasc Intervent Radiol 2003; 26:1–8.
13. Prince MR, Chabra SG, Watts R, et al. Contrast material travel times in patients undergoing peripheral MR angiography. Radiology 2002; 224: 55–61.
14. Cronberg CN, Sjoberg S, Albrechtsson U, et al. Peripheral arterial disease. Contrast-enhanced 3D MR angiography of the lower leg and foot compared with conventional angiography. Acta Radiol 2003; 44:59–66.
15. Leiner T, Ho KY, Nelemans PJ, et al. Three-dimensional contrast-enhanced moving-bed infusion-tracking (MoBI-track) peripheral MR angiography with flexible choice of imaging parameters for each field of view. J Magn Reson Imaging 2002; 11:368–377.
16. Fenlon HM, Yucel EK. Advances in abdominal, aortic, and peripheral contrast-enhanced MR angiography. Magn Reson Imaging Clin N Am 1999; 7:319–336.
17. Cloutier G, Soulez G, Qanadli SD, et al. A multimodality vascular imaging phantom with fiducial markers visible in DSA, CTA, MRA, and ultrasound. Med Phys 2004; 31:1424–1433.
18. Frayne R, Gowman LM, Rickey DW, et al. A geometrically accurate vascular phantom for comparative studies of x-ray, ultrasound, and magnetic resonance vascular imaging: construction and geometrical verification. Med Phys 1993;20:415–425.
19. Smith RF, Frayne R, Moreau M, Rutt BK, Fenster A, Holdsworth DW. Stenosed anthropomorphic vascular phantoms for digital subtraction angiography, magnetic resonance and Doppler ultrasound investigations. SPIE Phys Med Imaging 1994; 2163:235–242.
20. Fritz-Hansen T, Rostrup E, Larsson HBW, et al. Measurement of the arterial concentration of Gd-DTPA using MRI: a step toward quantitative perfusion imaging. Magn Reson Med 1996; 36:225–231.
21. Westenberg JJ, Wasser MN, van der Geest RJ, et al. Gadolinium contrast-enhanced three-dimensional MRA of peripheral arteries with multiple bolus injection: scan optimization in vitro and in vivo. Int J Cardiac Imaging 1999; 15:161–173.
22. Hernandez-Hoyos M, Orkisz M, Puech P, et al. Computer-assisted analysis of three-dimensional MR angiograms. Radiographics 2002; 22:421–436.
23. Westenberg JJ, van der Geest RJ, Wasser MN, et al. Vessel diameter measurements in gadolinium contrast-enhanced three-dimensional MRA of peripheral arteries. Magn Reson Imaging 2000; 18:13–22.
24. Boussion N, Soulez G, De Guise JA, et al. Geometrical accuracy and fusion of multimodal vascular images: a phantom study. Med Phys 2004; 31:1434–1443.
25. Foo TK, Ho VB, Hood MN, et al. High-spatial-resolution multistation MR imaging of lower-extremity peripheral vasculature with segmented volume acquisition: feasibility study. Radiology 2001; 219:835–841.
26. Madore B, Pelc NJ. SMASH and SENSE: experimental and numerical comparisons. Magn Reson Med 2001; 45:1103–1111.
27. Maki JH, Wilson GJ, Eubank WB, et al. Utilizing SENSE to achieve lower station sub-millimeter isotropic resolution and minimal venous enhancement in peripheral MR angiography. J Magn Reson Imaging 2002; 15:484–491.